EUCALL

The European Cluster of Advanced Laser Light Sources

Grant Agreement number: 654220

Work Package 6 – HIREP

Deliverable D6.4

EMP Compatible Stages

Lead Beneficiary: HZDR

Authors: Irene Prencipe, Alejandro Laso Garcia, Massimo De Marco, Mihail Cernaianu, Jakub Cikhardt, Fabrizio Consoli, Carsten Deiter, Jörn Dreyer, Marius Gugiu, Josef Krása, Alexander Pelka, Konstantin Sukharnikov, Andriy Velyhan, Tuomas Wiste, Joachim Schulz and Daniele Margarone

Due date: 30.09.2017
Date of delivery: 29.09.2017

Project webpage: www.eucall.eu

Deliverable Type	
R = Report DEM = Demonstrator, pilot, prototype, plan designs DEC = Websites, patents filing, press & media actions, videos, etc. OTHER = Software, technical diagram, etc.	R
Dissemination Level	
PU = Public, fully open, e.g. web CO = Confidential, restricted under conditions set out in Model Grant Agreement CI = Classified, information as referred to in Commission Decision 2001/844/EC	PU

This project has received funding from the *European Union's Horizon 2020 research and innovation programme* under grant agreement No 654220

Contents

This project has received funding from the *European Union's Horizon 2020 research and innovation programme* under grant agreement No 654220

1. Introduction

1.1 EMP generation in high power and high energy laser experiments

Intense broadband electromagnetic pulses (EMP) in the GHz to THz range are generated in the interaction of high intensity laser pulses and matter, in particular solid targets. When a high intensity laser pulse hits a sample, it couples to the electrons and accelerates a large number of them up to relativistic energies. The emission of THz radiation is attributed to the recirculation of hot electrons in the sample. A fraction of these electrons is ejected from the target. The resulting positive space charge drives return currents in the target holder structure that acts as an antenna and emits EMP in the GHz range. EMP can also be generated by charged particles propagating in the vacuum chamber, X-ray photoionization and other effects, even though no model accounts properly for all these processes. Experimental studies showed that the vacuum chamber acts as a resonance cavity and its geometry defines resonant frequencies in the EMP radiation (MHz range). EMP properties depend on a number of factors, including target geometry and composition, holder structure and material, chamber geometry and laser pulse properties.

EMP for PW-class laser facilities can have amplitude up to 100s kV peak to peak. Return currents can have amplitude up to 10s kA. Both return currents and radiated EMP can cause severe problems in electronic systems electrically connected to the target or positioned in and around the vacuum chamber, for example by introducing localized oscillating currents that can heat and damage sensitive components. Current techniques for damage prevention include shielding electronic components with Faraday cages; using shielded cables; switching off and electrically decoupling devices during the laser shot; placing any sensitive equipment far away from the interaction area; and ensuring a good isolation to the sample. With the upcoming high-repetition rate facilities, however, there is a large interest in understanding the EMP processes to better design crucial experimental parts that cannot be easily switched off or moved out of harm's way like target holders and detectors.

In particular, this report focuses on the current understanding of EMP generation and on the effects of EMP and return currents on high repetition rate precision positioning stages and other electronic components. Traditional mitigation strategies used for stages at lower repetition rates are not suitable for operation in the 1-10 Hz regime, because they are not reliable or not fast enough. For example, mechanical decoupling via relays currently used for controller protection is not reliable enough for high repetition rate operation and can cause further damage in the components due to arc discharging and current sparks.

1.2 Objectives

EMP resistant target positioning systems are currently used in laser facilities all over the world. Protection from EMP is usually achieved by insulating the target holder from the stages and by mechanically disconnecting motor controllers during shots with relays. However, mechanical decoupling is not advisable for high repetition rate operation (1-10 Hz) because relays are not always reliable in this operation regime and possible sparks could cause more damage than return currents flow through motors and controllers.

This project has received funding from the *European Union's Horizon 2020 research and innovation programme* under grant agreement No 654220

The scope of this activity is to provide indications on the compatibility of fast stages with electromagnetic pulses generated by high power and energy lasers and outlining strategies for avoiding destruction of stages, controllers and encoders.

More in detail, this activity is aimed at:

1. Providing an overview of the current understanding of EMP generation and EMP dependence on experimental parameters (see Section 2.1 and 2.2).
2. Illustrating EMP measurement systems (see Section 2.3).
3. Performing a systematic investigation of EMP level and EMP scaling at the DRACO laser facility, HZDR (see Section 2.4).
4. Completing a survey of EMP mitigation strategies currently used in operating research facilities and providing recommendations on EMP resistant precision positioning stages (see Section 3).

2. EMP generation: theory and experiments

The first part of our work was devoted to review current research activities on EMP in order to present an overview of the current understanding of EMP generation (Section 2.1) and EMP dependence on experimental parameters (Section 2.2). In Section 2.3, EMP and return current measurement instruments are described. Preliminary results of a systematic investigation of EMP levels at the DRACO laser facility are illustrated in Section 2.4.

2.1 EMP generation models

EMP generation mechanisms in different laser-matter interaction regimes are not completely understood. Different models have proposed. For short pulse lasers, EMP generation is intrinsically connected to the dynamics of relativistic (*hot*) electrons produced in the interaction between high intensity and high-energy laser pulses and a sample (Mora 2003). Only a small fraction of these hot electrons escape the target Coulomb potential creating a positive net charge, while the rest recirculates in the sample bulk (Hatchett 2002). Hot electron dynamics leads to the emission of a high frequency EMP component, in the THz regime. The current of hot electrons leaving the target is balanced by a background (*return*) current of non-relativistic electrons flowing to ground through the target holder. Therefore, dipole-like EMP radiation is generated by oscillating currents flowing through the holder and its support that act as an antenna (see Figure 1). This effect accounts for the GHz spectral range. This model applies to laser-matter interaction in the ps and sub-ps range (for instance to the case of the Eclipse laser, Dubois 2014, Poyé 2015a). Oscillating currents with amplitude up to 10s kA have been measured also in long pulse laser experiments (Cikhardt 2014, Kràsa 2017). Peak-to-peak amplitude of the EMP signal can reach 100s kV (Consoli 2010, DeMarco2014, Dubois 2014, Consoli 2015, Krása 2016, De Marco 2015, Poyé 2015a, and Poyé 2015b). Other sources of EMP are not accounted for by Poyé's model. The analysis of measurements and preliminary simulations related to nanosecond laser-plasma interaction indicates that low-frequency component of EMP signals is compatible with wakefields due to charged particles measured by time-of-flight detectors in experiments by Consoli and coworkers. It also shows that EMP should be affected by anisotropic particle emission from target, X-ray photoionization and charge implantation on surfaces directly

This project has received funding from the *European Union's Horizon 2020 research and innovation programme* under grant agreement No 654220

exposed to plasma (Consoli 2016). Resonant frequencies in the MHz range can appear in the EMP spectrum due to the onset of resonant modes in the vacuum chamber (acting as a resonance cavity). The resonant conditions determine how the signal can evolve in time after the initial radiation emission (Dubois 2014, Poyé 2015a, Poyé 2015b, De Marco 2016).

Albeit EMP in the THz frequency range is of extreme interest from the fundamental physics point of view, it does not affect electronics and stages. Therefore, the following discussion will focus on EMP emission produced by return currents and on the calculation of resonance frequencies in the vacuum chamber.

Numerical simulations and analytic models have been used to describe this process and investigate the correlation between EMP and experimental parameters. Large scale simulations are required to fully investigate EMP generation: particle in cell (PIC) codes simulate the dynamics of relativistic electrons, hydrodynamic codes simulate plasma expansion on longer time scales, Monte Carlo codes simulate electron propagation in the target bulk (Poyé 2015a). Numerical simulations are also used to calculate resonant frequencies in the vacuum chamber (Consoli 2015a, Consoli 2015b, De Marco 2016, COMSOL documentation). Due to the complexity of thorough numeric simulations of EMP generation, analytical and quasi-analytical models are required.

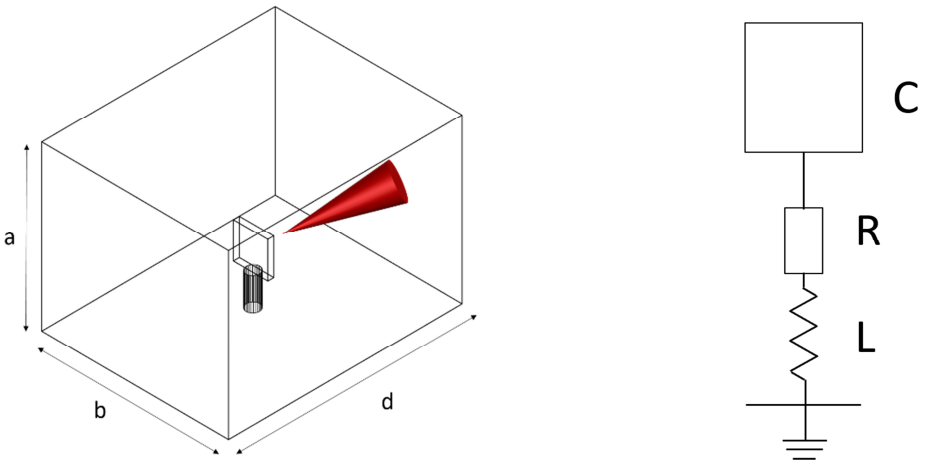

Figure 1: Schematic representation of a rectangular interaction chamber (size a x b x d) with target holder and incoming laser pulse (left). Electrical schematic of the antenna formed by the target and target positioning system (right).

The emission of electromagnetic waves from an antenna is related to the current flowing through the antenna by Ampère's law (see Section 3.2 for further detail) and, consequently, to the net charge produced by ejection of hot electrons. Therefore, EMP characteristics are strictly connected with the number and energy of electrons emitted during laser-target interaction. Hereinafter, we discuss a model developed by A. Poyé and coworkers to describe the target charging process and the dynamics of electron cloud (Poyé 2015a and Poyé 2015b). This is a useful tool to understand EMP generation, even though a number of approximations and hypotheses were required to keep the description relatively simple. Therefore, the model does not aim at providing a full and quantitative description of phenomena leading to EMP production. The model describes the charging process by

This project has received funding from the *European Union's Horizon 2020 research and innovation programme* under grant agreement No 654220

evaluating the number (N_h) and temperature (T_h), but also the radius (R_h) of the hot electron cloud. Three main processes are considered for calculation of N_h and T_h: laser heating; collisional cooling of hot electrons; and ejection of hot electrons from the target.

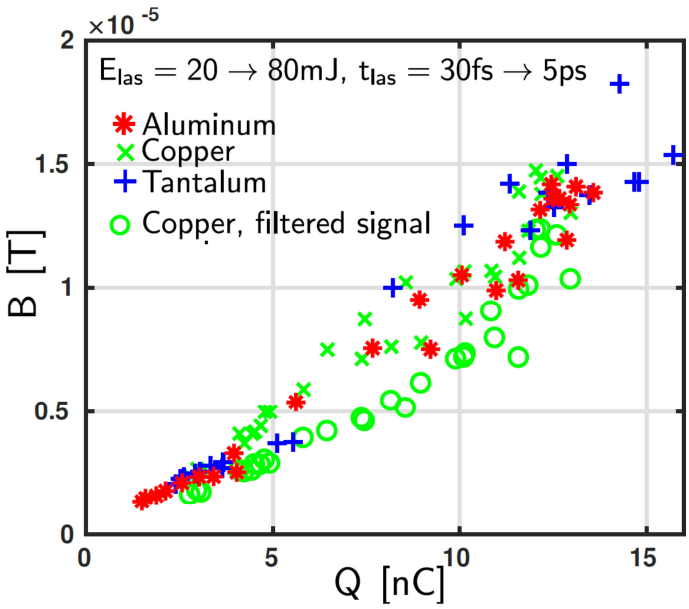

Figure 2: Correlation between magnetic field measured by a B-dot antenna and the corresponding charge accumulated on the target (calculated by integrating the return current signal). Courtesy of A. Poyé.

Laser heating generates hot electrons and sustains their temperature during the laser pulse. Laser properties define the hot electron number and energy. The hot electron average energy and temperature are assumed constant during the laser pulse, due to energy conservation.

Collisional cooling of hot electrons leads to energy transfer from the cloud of hot electrons to the target bulk. The characteristic timescale of hot-cold electron collision (t_{ee}) is defined as the mean free flight time of hot electrons: $t_{ee} = \frac{l_D}{v_{th}}$ (l_D is the electron diffusion length in the target, v_{th} is hot electron thermal speed). During the laser pulse ($t < t_{las}$), electron cooling takes place in timescales longer than t_{ee} (and it is only relevant for $t_{las} \gg t_{ee}$). Collisional cooling during the laser pulse leads to a reduction of the number of hot electrons and, as a consequence, of the total energy of the electron cloud. The temperature of hot electrons is sustained by laser heating and remains constant and equal to the initial value (T_0). After the laser pulse ($t > t_{las}$), the temperature of hot electrons decreases linearly.

Ejection of hot electrons modifies both T_h and N_h. Only electrons with energy higher than the potential barrier formed at the target surface are ejected. Therefore, calculation of the potential barrier is fundamental to evaluate the ejected current and the neutralizing return current. The effective potential barrier ($\Delta\Phi$) is calculated considering two effects: formation of an electron Debye sheath at the target surface (thermal potential) and net positive charge in the target (electrostatic potential). A detailed discussion of $\Delta\Phi$ calculation can be found in Poyé 2015b. The ejected current is

This project has received funding from the *European Union's Horizon 2020 research and innovation programme* under grant agreement No 654220

$$J_h = e\Omega_\beta n_{hot} \pi R_h^2 \int_{|e\Delta\Phi|}^{\infty} f_h v \, d\epsilon$$

where

- e is the elementary charge
- $\Omega_\beta = (1 - \cos\beta)/2$ is the fraction of electrons propagating in a direction compatible with electron ejection, β is the half angle of the electron ejection cone
- n_{hot} is the density of hot electrons
- $f_h(\epsilon, T_h)$ is the energy distribution function of hot electrons, that in this model approximation is described by a Maxwell-Jütner function.
- v is the electron speed
- ϵ is the electron energy.

These equations only apply to the case of targets with thickness larger than range of electron propagation in the target itself. For thinner targets, hot electrons moving towards the rear target surface are not necessarily stopped in the target due to collisions: a Debye sheath of hot electrons is formed also on the backside of the target and a fraction of hot electrons actually escapes the target from the rear surface. The fraction of ejected electrons changes from Ω_β to $\Omega_{\beta,forward} + \Omega_{\beta,backward}$. Hot electrons at the rear surface contribute to both the thermal and electrostatic potential. These effects can be taken into account by calculating the ejected current as $J_h = J_{h,front} + J_{h,rear}$ and by modifying the electron distribution function accordingly.

Based on the model developed by A. Poyé and coworkers, three different regimes can be identified for target charging depending on laser pulse duration: (i) full (quasi-instantaneous) ejection regime, (ii) quasi-stationary regime, and (iii) thermal (intermediate) regime. The timescales mentioned hereinafter refer to the following laser parameters: laser energy $E_{las} = 0.8\,J$, laser wavelength $\lambda = 800\,nm$, focal spot radius $r_{las} = 6\,\mu m$ and laser to hot electron energy transfer efficiency $\eta_{las} = 0.4$.

Full ejection regime ($\overline{<\epsilon>} > \overline{|e\Delta\phi|}$). For very short pulse durations, the cloud of hot electron has usually higher temperature ($T_h = T_0$) because of the higher laser intensity and because no collisional cooling takes place during the laser pulse. The potential barrier is low due to the low electron density (reduced thermal potential) and to the low total number of hot electrons N_{tot} (reduced electrostatic potential). Therefore, the average electron energy ($<\epsilon>$) is higher than the potential barrier ($|e\,\Delta\phi|$) and all hot electrons generated in the interaction are ejected from the target almost instantly. In this regime, the total ejected charge can be approximated as $Q \approx eN_{tot}$. For the above-mentioned laser parameters, this regime occurs for pulse duration lower than 10 fs.

Quasi-stationary regime ($t_{las} > t_{cool}$). For pulse durations longer than the cooling time (time required for the hot electron temperature to drop to 0.01 T_0), the hot electron cloud is sustained by the laser and the electron temperature is kept constant at T_0. In this regime, the thermal potential is constant and electrostatic potential reaches a steady state when an

This project has received funding from the *European Union's Horizon 2020 research and innovation programme* under grant agreement No 654220

equilibrium is reached between hot electron production and electron energy dissipation. The ejected current is therefore constant

$$J_h \cong -\Omega_\beta e \frac{N_{tot}}{t_{las} < v >_0} \int_{|e\Delta\Phi|}^{\infty} f_h(\epsilon, T_0) v \, d\epsilon$$

where $< v >_0$ is the hot electron average speed for $T = T_0$. In this regime, the total ejected charge can be approximated as $Q \approx J_h t_{las}$. For the above-mentioned laser parameters, this regime occurs for pulse duration longer than 500 fs.

Thermal regime. This regime occurs for intermediate time durations, shorter than the cooling time but long enough for the intensity to be too low for full ejection. In this regime, a fraction of the hot electrons is trapped by the target potential and the dynamics of electrons in the target leads to EMP production also on timescales longer than the laser pulse duration. No further approximations can be considered to simplify the description of this intermediate regime.

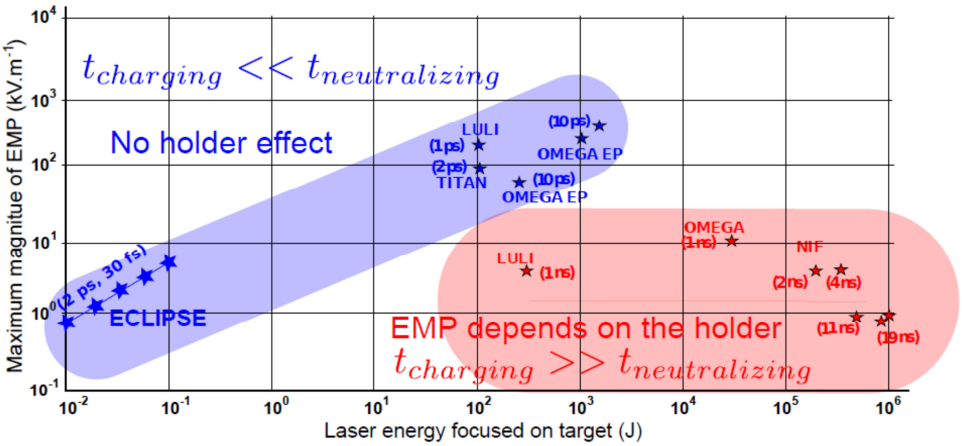

Figure 3: Effect of the holder configuration on EMP emission (from Poyé 2015b). Reprinted figure with permission from Poyé 2015b (https://doi.org/10.1103/PhysRevE.92.043107). Copyright 2015 by the American Physical Society.

Once the current of hot electrons and the charge accumulated on the target have been calculated, the holder geometry and electrical connection to ground need to be taken into account. In the simplest case, the target is a disc supported by a stalk that also acts as connection to a ground plate acting as a mirror (Dubois 2014 and Poyé 2015a). In the far-field approximation, this target support configuration can be approximated as a half wave dipole antenna with characteristic emission frequency, $f = \frac{c}{2l_{tot}} = \frac{c}{4(l+\frac{\pi d}{2})}$, where l_{tot} is the total antenna length and is calculated as the sum of the length of the stalk l and half target perimeter (d is the target diameter). The characteristic frequency calculated in this approximation is in very good agreement with the experimental result (Poyé 2015). In addition, in this case, the holder inductance is large enough to delay return currents and avoid neutralization during electron ejection (this process is not accounted for in the model presented in this section). For more complex holder geometries, calculation of characteristic

This project has received funding from the *European Union's Horizon 2020 research and innovation programme* under grant agreement No 654220

EMP frequencies is not so straightforward and return currents from ground can take place in shorter timescales (depending on the holder configuration). In general, if the charging time is larger than the neutralization time, target charging and EMP emission are strongly affected by the holder configuration (see Figure 3).

The model developed by Poyè and coworkers is relatively simple and robust and takes into account some of the most relevant processes involved in EMP generation. However, the model has been validated only in short pulse (in the ps regime) and low energy experiments (< 100 mJ), i.e. for intensities well below the relativistic threshold (10^{18} W/cm^2). Therefore, experimental validation for long pulse, high-energy lasers would be needed, together with a more comprehensive model taking into account relativistic effects.

After EMP is emitted, the vacuum chamber acts as a resonance cavity. Resonant frequencies are visible in EMP spectra and need to be calculated to support interpretation of experimental results. The resonant frequencies as well as the leakage time of EMP energy are directly related to the shape and structure of the chamber (DeMarco 2016) and to optics and components present in the chamber itself that can lead to resonance at harmonics. This makes evaluation difficult for EMP effects expected for a specific experimental condition using data collected from any other experimental configuration or facility. This is a critical issue because an evaluation of the expected EMP signal is required when planning a high power laser experiment in order to avoid possible problems for electronic devices, which could even lead to a loss of experimental data (Brown 2010, Brown 2012).

The characteristic frequencies in the vacuum chamber are usually calculated via finite element methods, that keep into account the chamber geometry and the components mounted in the chamber. A simpler approach can be used for approximate calculation of resonant frequencies simply by considering resonant cavity equations. For example the resonance frequency of TE and TM modes in a rectangular cavity is

$$f_{mnl} = \frac{c}{2\sqrt{\mu_r \epsilon_r}} \sqrt{\left(\frac{m}{a}\right)^2 + \left(\frac{n}{b}\right)^2 + \left(\frac{n}{d}\right)^2}$$

Where m, l, n are the mode numbers and a, b, d are the corresponding dimension (see Figure 1); and μ_r and ϵ_r are the relative permeability and permittivity of the medium present in the chamber. This approach was used, for example, by Mead and coworkers to interpret EMP signals measured in the rectangular Vulcan PW laser chamber (Mead 2004).

2.2 Experimental investigation of EMP

Experimental investigation of EMP generation mechanisms and EMP dependence on laser and target parameters is relatively recent. Systematic studies have been often performed with low power lasers, while results of experiments performed in high power and energy laser facilities are often parasitic. Therefore, dedicated experiments would be needed to study parametric dependence of EMP generation on laser and target parameters and to better understand EMP generation mechanisms in the relativistic regime.

In general, experimental investigation of EMP emission is performed by measuring the EMP signal with B-dot and D-dot antennas over several 100s of ns. This measurement is also

This project has received funding from the *European Union's Horizon 2020 research and innovation programme* under grant agreement No 654220

fundamental to evaluate EMP hardness of electronic components. Another crucial information to be correlated with the EMP power spectrum is the measured value of return current flowing from target to ground. Probes and methods used for such measurements are described in Section 2.3. Hereinafter, we discuss some interesting experimental results from literature.

EMP emission has been investigated experimentally as a function of laser parameters. Laser pulse energy and duration are the parameters that most influence EMP emission. Figure 4 shows the ejected hot electron charge as a function of these two parameters for a low energy (< 100 mJ) and short pulse (< 10 ps) regime. In this regime, Poyè's model shows very good agreement with experimental results: the ejected hot electron charge increases with the laser pulse energy and is reduced for longer pulses. Return currents in the kA regime and significant EMP generation (100s kV/m) have been measured for longer laser pulses and higher laser energies for example at PALS, Vulcan and Titan (Cikhardt 2014, Kràsa 2017, De Marco 2017, Eder 2009). Peak EMP measured at Titan with a high frequency B-dot probe for 0.6 ps, 2 ps and 20 ps show a clear increase as a function of the laser pulse energy (400 kV/m for about 330 J and 2 ps), while the dependence on pulse duration is less clear (Eder 2009). In general, no clear dependence of EMP signal has been observed from pre-plasma properties, laser intensity and position in focal direction. Most of these results have been observed in parasitic experiments and are still unpublished.

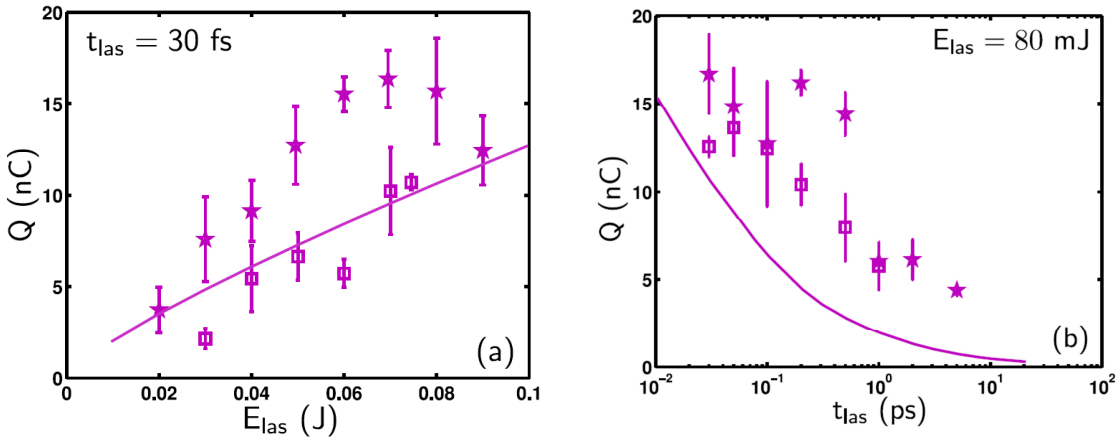

Figure 1: Charge ejected from Teflon targets measured with the Eclipse laser (CELIA) as a function of pulse laser pulse energy (left) and duration (right) compared with Poyé's model. Reprinted figure with permission from Poyé 2015b (https://doi.org/10.1103/PhysRevE.92.043107). Copyright 2015 by the American Physical Society.

EMP generation can show a strong dependence on target composition and geometry and on the target holder configuration (see Section 2.1). In general, materials with different atomic number and work function show different laser absorption and hot electron generation, thus influencing EMP emission. Moreover, different materials can have different chemisorption properties, leading to differences in the composition and quantity of contaminants present on the target surface (Krasa 2015).

This project has received funding from the *European Union's Horizon 2020 research and innovation programme* under grant agreement No 654220

Only slight differences (and no clear trend) were observed at the Eclipse CELIA facility (20-80 mJ, 30 fs-1ps) between targets made of Cu, Ta and Al. A significant difference could be expected with Teflon targets, but the ejected charge is comparable with the metallic targets (see Figure 4). However, the drop in ejected charge is much faster for Teflon targets with respect to metal targets. This is attributed to the higher electrostatic potential building up in insulating materials (Dubois 2014, Poyé 2015a, Poyé 2015b).

A recent experimental campaign showed that EMP signal measured for solid H targets (Garcia 2014) is more than one order of magnitude lower than the signal measured for standard Cu foils. In this case, the dependence on laser energy is not so relevant and measured values are probably within the shot-to-shot fluctuations (De Marco 2017).

EMP frequency and amplitude measured at the DRACO facility for laser-driven electron acceleration showed a strong dependence on the type of target: gas jet or gas jet with ~100 µs thick Al foils (results are illustrated in more detail in Section 2.4). This is due to the different EMP generation mechanisms in solid and gas targets. In the latter case, EMP generation can be attributed to the dynamic of accelerated electrons.

EMP emission also shows strong dependence on the target geometry and size. In general, return currents and EMP signal increase by 30% or more for target thickness in the µm range with respect to 1 mm thick targets, as demonstrated by Raczka and coworkers for laser pulses with energy up to 92 mJ and duration around 40 fs (Raczka 2017). Also target substrate dimensions and material plays an important role in EMP emission: EMP signal measured at CLF Vulcan using targets with reduced lateral size (3 mm) is less than one third of the signal measured for 8 mm wide targets (laser energy between 50 and 750 J), (D. Carrol 2017). Target shape influences strongly electron dynamics and return currents. This is the case, for example, of reduced mass targets (Zeil 2014) and targets grounded through a coil (Kar 2016). EMP generation from targets supported by stalks shows a strong dependence on the stalk geometry and material. The amplitude of radiated EMP decreases with decreasing holder material conductivity and with increasing target support length (as observed at CLF by D. Neely and coworkers). Since target neutralization occurs primarily via surface discharge phenomena, target stalks with a length and shape maximizing the holder conductance reduce significantly EMP emission (P. Bradford et al, in preparation).

2.3 EMP measurement systems

Experimental investigation of EMP requires a collection of current probes to measure currents flowing through the target and of B-Probes and D-Probes to measure magnetic and electric fields in different positions in the vacuum chamber (i.e. at different distances from the target and under different angles) (Consoli 2003, Cikhardt 2014, De Marco 2015, De Marco 2016). Vacuum compatible antennas are required to measure EMP in the interaction chamber, while non-vacuum compatible antennas can only be used around the vacuum chamber (where the EMP field is attenuated of about two orders of magnitude).

This project has received funding from the *European Union's Horizon 2020 research and innovation programme* under grant agreement No 654220

B-dot antennas are instruments sensitive to the variation of the magnetic field with time dB/dt (or $\dot{B}$, hence the name). The standard structure of such antenna is a wire forming a loop. With this structure, the antenna is sensitive to the magnetic field perpendicular to the plane of the loop. Details about the usage of such devices can be found at [add citations].

D-dot antennas receive their name in an analogue fashion to B-dots. They are devices sensitive to the variation of the electric field dD/dt (or $\dot{D}$).

In both these antennas, the voltage at the output can be related to the field via the transfer function. For example, in the case of the B-dot sensor:

$$V_0 = Z\, A_{eq} dB/dt$$

Where V_0 is the voltage at the output (for example as seen by an oscilloscope), Z is the impedance of the system, A_{eq} is the transfer function and dB/dt is the field being measured.

In a similar way, a B-dot antenna can be used to measure the current flowing through a wire or cable. This application can be extended to return current in laser interactions by making the current flow through a cylindrical section and having the B-dot antenna measure the magnetic field generated by such current. In this case, the return current is related to the magnetic field via Ampere's law:

$$\oint_S \vec{B} \cdot d\vec{s} = \mu_0 I$$

Where $\vec{B}$ is the magnetic field, ds is the surface element through which B passes, μ_0 is the magnetic permeability of vacuum and I is the current flowing through the wire. A schematic for such a measurement is show in Figure 6a.

High return currents neutralizing the positive charge occurred on an irradiated target can be measured with the use of resistive and inductive probes (Benjamin, Cikhardt). The resistive probes need careful electromagnetic screening against EMP produced within the target chamber and must be free from inductance and capacitance to detect unperturbed target signal. Since the frequency spectra of the target current range up to GHz domain, mainly a low inductance of the resistive probe can strongly disturb the target signal.

This technical problem has been solved by employing the newly developed inductive probe, the copper shielding of which avoids picking up EMP signal by a small loop antenna detecting

This project has received funding from the *European Union's Horizon 2020 research and innovation programme* under grant agreement No 654220

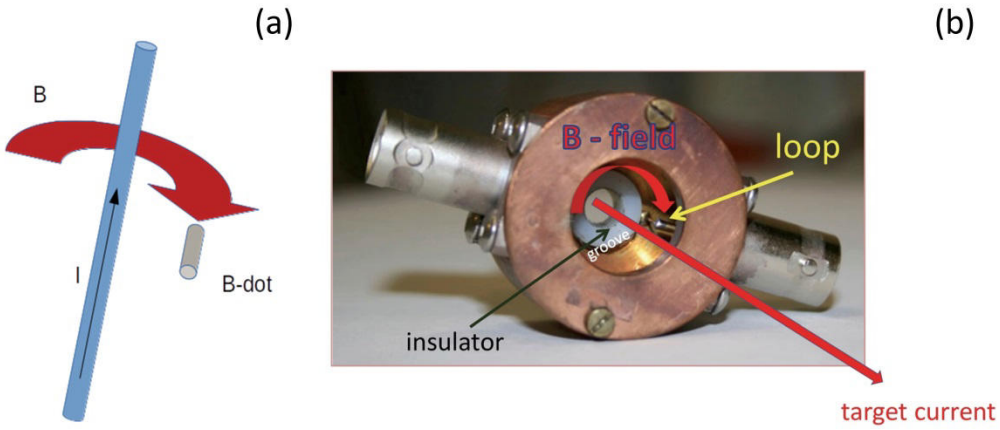

Figure 2: Use of a B-dot probe for current flow measurement (a). Example of a newly developed inductive target probe (b). The loop antenna is localized within the groove. The copper cylinder avoids picking up EMP signal produced within the target chamber.

magnetic field induced by the neutralizing target current, as Figure 6b shows. The inductive probe measures a short circuit current flowing between the target crater and grounded chamber through a target holder and, thus, does not influences the target current as the resistive probe. A schematic for such a measurement is show in Figure 6a, and a newly developed probe is presented in Figure 6b.

Conductive probes described so far are intrinsically derivative devices, so current is proportional to the time derivative of the incoming fields. The spectrum is thus proportional to frequency, and high frequency components are naturally amplified with respect to the low frequency ones. Conductive probes can also create local perturbations in the local electric field. In addition, these probes require electrical signal to be transported to an oscilloscope (usually positioned in a Faraday cage out of the chamber) through conductive cables. These cables albeit shielded can pick up additional EMP noise reducing significantly the signal to noise ratio and making data interpretation more difficult. An innovative way of measuring EMP while overcoming these limitations makes use of electro-optic probes developed by Consoli et al. (Consoli 2016, Robinson 2017). This method is based on the Pockels effect: the polarization of an incoming probe beam is rotated in KDP or BSO crystals if an electric field is applied along the crystal axis. The phase rotation is directly proportional to the electric field E_L

$$\Delta\theta = \frac{2\pi}{\lambda_0} n_0^3 r_{63} L E_L$$

Where λ_0 is the wavelength of the probe beam, n_0 is the linear refractive index of the crystal, r_{63} is the electro optic permittivity. An adjustable polarizer is positioned downstream, so that the phase rotation can be related to the intensity of the transmitted probe beam that is transmitted through multimode optic fibers and measured with photodiodes. Thee crystals positioned along mutually orthogonal axes allow measurement

This project has received funding from the *European Union's Horizon 2020 research and innovation programme* under grant agreement No 654220

of all three components of the electric field. This diagnostic is schematically illustrated in Figure 7. As illustrated by recent works, the use of electro-optic probes has shown the importance of the low frequency part of the spectrum, also compared to the high frequency signal. A modified version of this probe, making use of a magneto-optic crystal, allows magnetic field measurement.

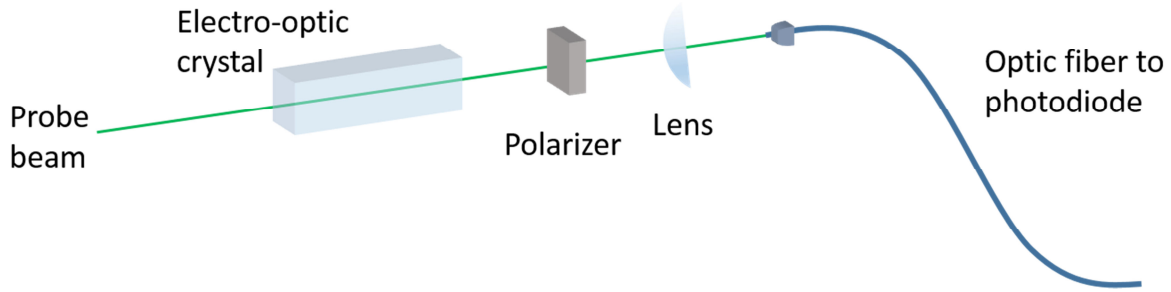

Figure 3: Schematic representation of an electro-optic diagnostic for EMP as described in Robinson 2017. A more compact and versatile version of the electro-optic diagnostic can be found in Consoli 2016.

Hereinafter, we report a list of antennas used by EUCALL partners for EMP measurement.

ELI-Beamlines

1. homemade loop B-Probe, 2 cm diameter small loop probe calibration up 1GHz, not compatible with vacuum, for use in vacuum glass or ceramic bulbs would be needed to insulate the probe from vacuum.
2. homemade Moebius Loop Magnetic Field Sensor, 1 cm diameter coaxial loop probe calibration up to 1GHz, vacuum compatible, compatible with ionizing radiation (lower background/noise), coaxial cables (RG-142 B/U 4.95 mm PTFE 50 Ohm) used for operation in vacuum, Sn60Pb40 used for soldering.
3. 2 commercial Rohde & Schwarz B-probes, 2 cm diameter small loop probe, calibrated from 50MHz to 1GHz, not compatible with vacuum; for use in vacuum glass or ceramic bulbs would be needed to insulate the probe from vacuum (collaboration with J. Krasa's group CAS and PALS).

ELI-ALPS

1. HE300 KIT RF-antenna. Set of 4 antennas: not vacuum compatible. Aim: probing enviroment around target chamber, 9 kHz to 7.5 GHz.
2. EZ-17 Current probe. Aim: probing current in power, driver and signaling cables. 20 Hz to 100 MHz, max. 300 A.
3. HZ-14 Near field probe set. (2 H-field + 1 E-field.). Aim: measuring RF emission from PCB, cables, and shielded enclosures, 9 kHz to 2 GHz.

Helmholtz-Zentrum Dresden-Rossendorf

1. Homemade broadband antennas can be used to measure the EMP field in a single orientation. The antennas currently in use cover the range of frequencies up to 10 GHz (the current limit on frequency is at 5GHz due to oscilloscope limitations).

This project has received funding from the *European Union's Horizon 2020 research and innovation programme* under grant agreement No 654220

2. Homemade B-Dot antennas measure the EMP field in a single orientation. They are compact and can be arranged easily to measure different orientations.

Other commercially available antennas are commonly used in EMP experiments, for example Prodyn B-dot probes. These antennas are normally calibrated, cost of a few 1000s €/probe and are widely used. In general, the use of calibrated commercially available antennas could enable easier comparison of EMP characteristics between different facilities.

In general, the response of antennas need to be calibrated. Cross-calibration with calibrated antennas is an option, especially when multiple antennas are used in the same experiment to characterize EMP in different positions. On the other hand, a cable loop connected to an oscilloscope with appropriate attenuators is enough for qualitative measurement aimed at analyzing component failure modes.

2.4 Systematic studies of EMP level at DRACO (HZDR)

Several experiments were performed at the Dresden laser acceleration source (DRACO) facility to determine the most suitable way of measuring the EMP and its relation to electronic devices. A preliminary test was performed using B-dot probes provided by ELI-Beamlines and by the Institute of Physics of Prague in the frame of the EUCALL project. This test involved HZDR, ELI and European XFEL researchers. The results presented hereinafter only refer to experiments performed with HZDR homemade probes (described in Section 2.3).

The DRACO laser is a Ti:Sapphire laser with double chirp pulse amplification capable of delivering up to 45 J pulses with a short pulse duration of 30 fs. The beam can be focalized down to a few micrometers allowing for intensities of 10^{21} W/cm^2. Two different experimental areas can currently be used: an ion acceleration area where relativistic laser-plasma interaction with solid targets is used, and an electron acceleration area where the laser pulse interacts with gas jets allowing the study of laser wake field acceleration and under-dense plasma physics.

Measurement of EMP at DRACO ions

Two broadband antennas were used in parasitic mode at the DRACO ion interaction area. The laser parameters were an energy of 2 J, 30 fs pulse duration and a few micron focal spot. The antennas were placed outside the chamber, one at target normal position and the other at an angle of 45° with respect to the target normal direction. Different targets were studied comprising aluminium foils and carbon nano-foams, as well as the dependence of the signal with the laser intensity.

The antennas were placed at the output of two flanges of the interaction chamber, each one at the specified angle. The signal was then routed through 4 m long double shielded cables. The cables were connected with a 20 dB attenuator each to a fast digital oscilloscope (4 GHz, 20 Gs/s).

This project has received funding from the *European Union's Horizon 2020 research and innovation programme* under grant agreement No 654220

An example of such measurement is shown in Figure 8. The left panel shows a typical signal recorded by the antenna located at target normal. The peak-to-peak amplitude is approximately 20 V and it lasts for hundreds of nanoseconds after the pulse arrival. On the right panel the frequency components are shown. The main component corresponds to a peak of 1 GHz, with sometimes a secondary peak at f~1.4 GHz.

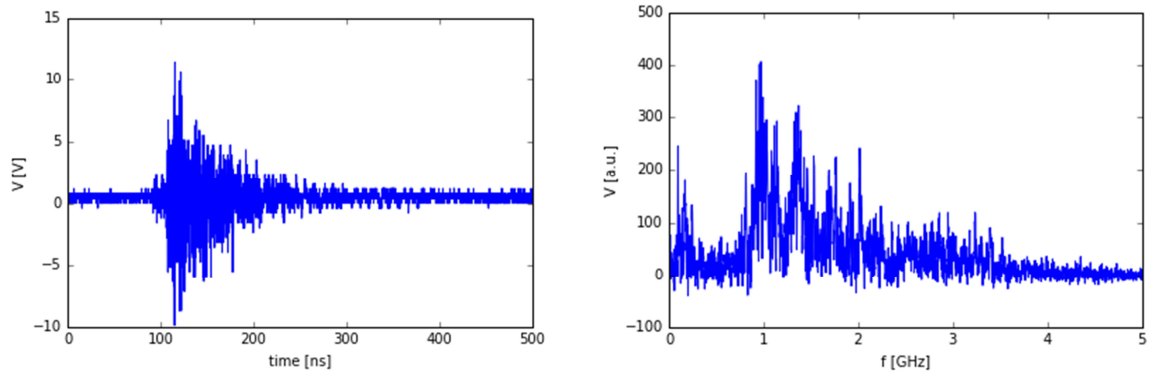

Figure 8: Left: trace recorded by an oscilloscope corresponding to the EMP measured by a broadband antenna. Right: frequency components of that signal.

Measurement of EMP at DRACO electrons

A similar setup was employed at the DRACO electron acceleration area. In this case, two broadband antennas and two Mobius loops were used to measure the EMP field. One of the antennas was placed on top of an electronic rack, which experienced EMP issues at certain experiments (antenna A, Figure 9, top left). The other broadband was located on the beam axis, approximately 10 cm under it (antenna B, Figure 9, top right). The Mobius loops were placed immediately in front of the latter antenna (antennas C and D, Figure 9, bottom left).

The analysis of this data is still ongoing at the time of writing this report. As an example, Figure 10 shows the results of antenna B for shots on the gas jet only and on the gas jet with two 100-µm thick aluminum foils positioned about 100 µm downstream with respect to the gas jet. The signal corresponding to a gas jet only shot presents a low frequency spectrum as opposed to the high frequency visible in the gas jet + Al foil shot. Specifically, the gas jet + Al foil shot indicated that the high frequency component is superimposed on top of the gas jet signal. This effect can be seen at the 150-200 ns signal trace. The amplitude of this signal is roughly a factor 2-3 smaller than the one obtained at DRACO ions.

This project has received funding from the *European Union's Horizon 2020 research and innovation programme* under grant agreement No 654220

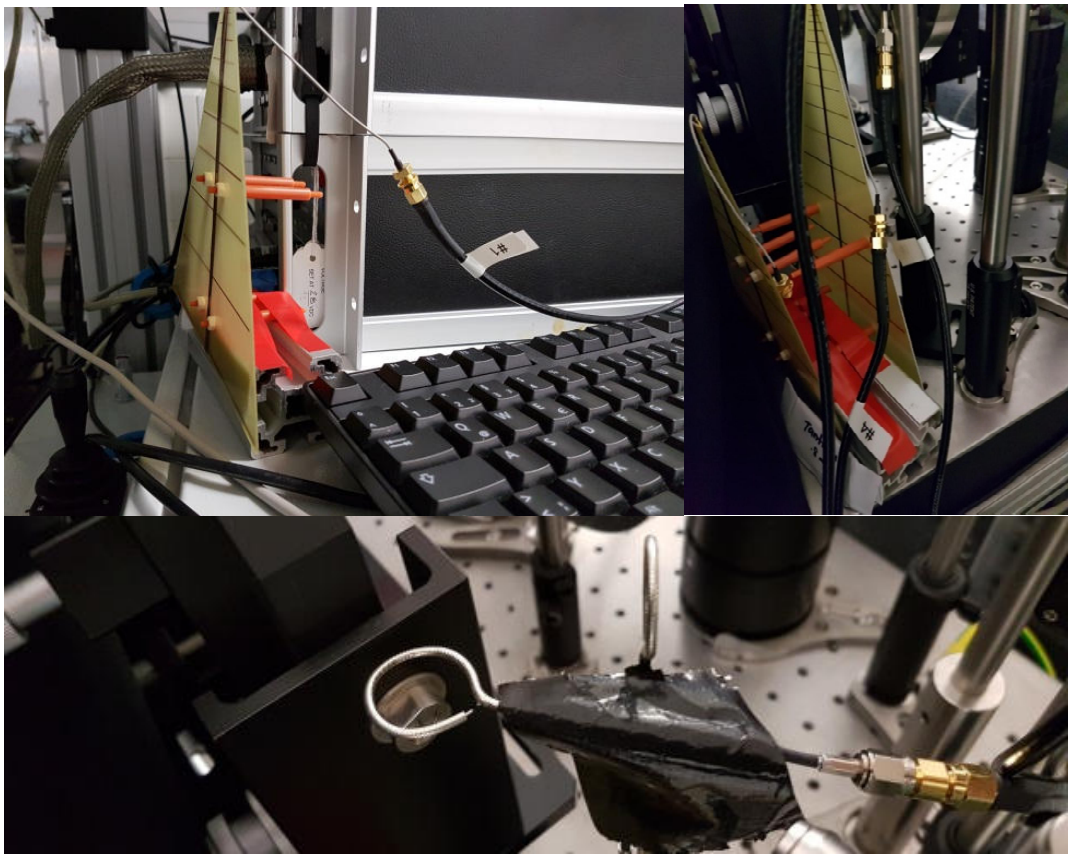

Figure 9: Top left: broadband antenna (antenna A) on top of an electronic rack. Top right: broadband antenna (antenna B) 10 cm under beam axis. Bottom: Mobius loop antennas (C and D) in front of antenna B.

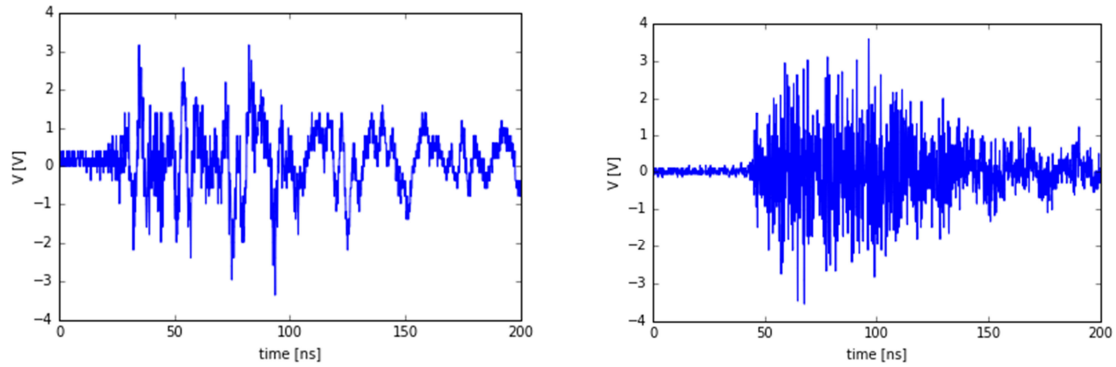

Figure 10: Left: trace recorded on a gas jet only shot. Right: trace recorded on a gas jet and Al foil shot.

Summary of the results.

In general, these tests were the first steps to develop permanent measuring stations with which characterize the EMP signals at DRACO experiments. Qualitative results could be obtained with homemade antennas, for a quantitative analysis antenna calibrations are needed.

This project has received funding from the *European Union's Horizon 2020 research and innovation programme* under grant agreement No 654220

Effects on the cables outside the chamber have proven to be negligible when measuring EMP; the same must be proven for cables placed inside the chamber. A small EMP pickup signal was also observed on the oscilloscope itself, indicating the need of additional shielding.

The challenge of measuring EMP inside the chamber in a quantitative manner is complex: the very high electric fields (kV/m), the effect of all the elements in the chamber perturbing the field, the electromagnetic pickup in the cables and the need of suitable vacuum-compatible and calibrated probes are hurdles that must be overcome.

3. EMP mitigation strategies and EMP resistant stages

In this Section, we present an overview of EMP mitigation strategies currently used in operating research facilities for target positioning systems and other electronic devices. We also describe EMP protection measures discussed in the frame of the HIREP WP and adopted for the target positioning system of the ELI-MAIA interaction chamber at ELI-Beamlines.

Correct operation of stages and controllers can be affected by two effects: (i) charge build-up in specific regions of the positioning system and consequent discharges though motors and controllers (static or low frequency); (ii) and radiated EMP (high frequency).

In general, radiated EMP can be minimized with an appropriate design of the target holder and positioning system. One possibility is designing the holder so that oscillating currents in the holder are damped as quickly as possible. Appropriate holder design is also a key aspect to avoid return current damage in stages and controllers. In general, for low repetition rate facilities, protection from EMP is achieved by insulating the target holder from the stages and by mechanically disconnecting motor controllers during shots with relays. These mitigation strategies are not optimal for operation in the 1-10 Hz regime. Mechanical decoupling via relays is not reliable and fast enough in this regime. A check on relay correct operation would be needed before each shot to make sure that all the relays are disconnected at the right time (possible resonances could cause the relays to open/close at the wrong time). In addition, charge build-up in the relays during the disconnection phase could produce arch discharges. Current spikes due to arch discharges are potentially more dangerous than return currents for motors and controllers.

Another possible solution is the definition of an alternative ground path (a *lightning rod system*) to guide safely return currents eliminating the need of mechanically disconnecting motors and controllers. Controllers can be protected by unexpected currents with spark gaps or diodes. This solution has been adopted at Phelix GSI. At GSI, industrial controller units (Beckhoff) are located in switchboards with protective diodes that provide grounding when the potential is too high. A lightning rod system is used to avoid charge build-up. For moving parts, contact is provided by a brush of conductive material. Target positioning stages are positioned below the chamber main breadboard, on a lower plane, and are grounded to this lower breadboard. Flow of return current through the motors is avoided with a post of insulating material between target holder and target positioning stages. No encoders nor

This project has received funding from the *European Union's Horizon 2020 research and innovation programme* under grant agreement No 654220

end switches are used because protection of input circuits is very hard to achieve. Encoder operation requires low-frequency (Hz-kHz) level changes (few V) which makes them sensitive to bursts or spikes and thus tend to produce more counts in noisy environments. Therefore, the mechanical system should not rely on them to move (which would be the case when using DC motors or friction-based piezo motors). However, online feedback on the stage position is required for high repetition rate operation in order to ensure correct target positioning for each shot and stop laser operation in case of motor malfunction (due for example to electrical failure, friction due to debris, bumping by personnel, mechanical blocking…).

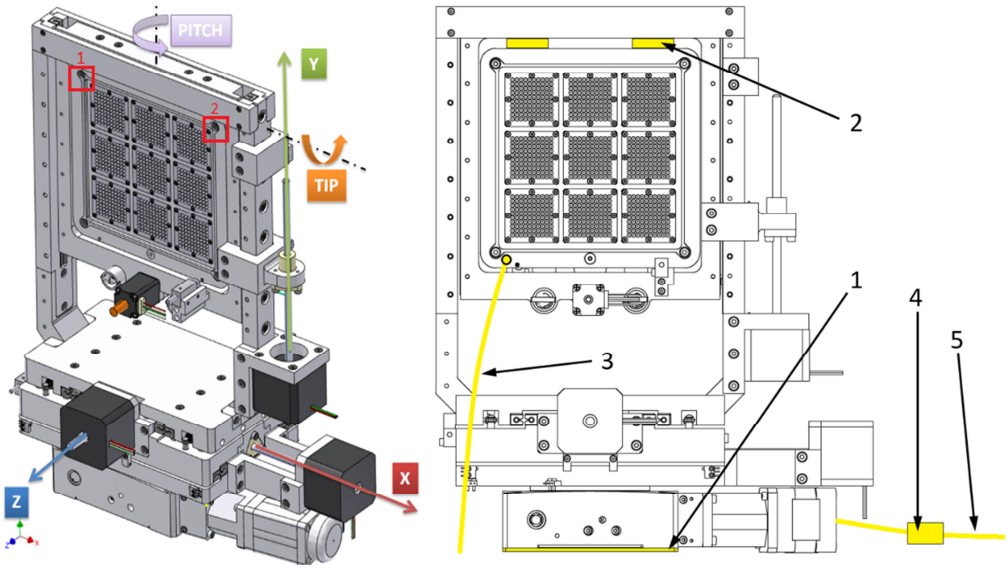

Figure 4: ELI-MAIA target positioning system (left). EMP protection precautions (right): 1. PTFE Baseplate 2. PEEK flexures 3. Target plate grounding 4. Relay 5. Cables encased in copper braid.

EMP protection strategies for the ELI-MAIA target positioning system have been devised in the frame of the HIREP work package (see Figure 8). The ELI-MAIA target-positioning tower offers 5 degrees of freedom, with 1.5 µm resolution for the degree of freedom used in focusing (along the laser axis) and is able to perform at 10 Hz. The target positioning system is insulated from the breadboard with a polytetrafluoroethylene (PTFE) baseplate. The baseplate discourages electrical current from travelling through the portion of tower attached to actuators. Polyether ether ketone (PEEK) flexures ensure target insulation. The degree of freedom that immediately precedes the target holder is fabricated from insulating material. The target plate is directly grounded to the interaction chamber. Mechanical decoupling during shots is foreseen for each cable via relays. All cables are shielded and additionally surrounded by copper braided sleeving material.

Motor controllers and other electronic devices (including scopes, computers, detectors, and cameras) need to be protected by radiated EMP with frequency in the MHz-100s GHz range. In general, two strategies can help mitigating effects of radiated EMP: increasing the component distance from the interaction chamber (EMP amplitude is inversely proportional to the square of the distance); and shielding components with Faraday cages. An example of Faraday cage specifically designed for EMP protection of a component is the Faraday cage

This project has received funding from the *European Union's Horizon 2020 research and innovation programme* under grant agreement No 654220

used at GSI for cameras. The component is encapsulated in an Al housing with copper rings to avoid air gaps around the opening for the camera objective. Metal-coated filers are often used in front of the objective to complete the shielding (needed especially if the camera looks directly at TCC). Metal grids can be used instead of the Al housing. No currents are supposed to flow between inside and outside the box, besides the camera power supply. A transformer is positioned in the cage for AC to DC conversion. Camera trigger and output signal are transmitted via optic fibers. Everything in the cage is insulated from the box itself and the box is grounded to the breadboard. Generally, old analogic equipment (for example oscilloscopes) is much more resistant to EMP than more recent digital equipment.

Cables in the vacuum chamber can act both as receiving and emitting antennas. Unwanted currents induced by EMP in the cables can damage electronic components. Cables and other conductive materials in the chamber can also pick up the EMP signal and emit EMP at different characteristic frequency. Therefore, cable shielding is extremely important. For example, homemade cables made using Teflon for insulation isolation and a metal mesh for cable shielding are used at GSI. Other laser facilities use similar cables available on the market.

4. Synergy aspects and future perspectives

The synergy between EUCALL partners in HIREP has been a key factor for the activity on EMP. The group was formed by experts with different background and experience allowing the formation of a very productive collaboration that will most likely extend to future activities beyond the end of the EUCALL project. For example, HZDR staff contributed to the design of target holder insulation for the ELI-MAIA beamline at ELI-Beamlines and ELI-Beamlines researchers supported the HZDR group in the development of antennas and return current measurement systems. In addition, parasitic experiments have been performed at HZDR using or testing equipment from other EUCALL partners (European XFEL, ELI-Beamlines). The complementary experience of researchers from different facilities was also very helpful for the collection of information on EMP generation and mitigation discussed in this report.

This report has been produced as a collaboration between EUCALL and non-EUCALL EMP experts, partially as a result of the HIREP-EMP Workshop held at HZDR, Dresden, on August 28-29th 2017. Contributions from a large number of partners are crucial when EMP mitigation strategies are considered because extensive competences are available at operating facilities from day-to-day operation experience. These data and results are in general not published; therefore, knowledge about EMP mitigation is often anecdotal. The lack of an overview on EMP generation and mitigation has be acknowledged during the workshop, leading to the decision of forming a broader collaboration aimed at the production of a review paper on these themes.

Finally, a very promising outcome of this activity is the preparation of a joint proposal of an EMP dedicated experiment at Draco 150 TW/1 PW laser, HZDR. The proposed experiment would be led by the HZDR team and involve both EUCALL and external partners and focus on the correlation between radiated EMP and return currents for different target types, holder geometries and laser parameters. This would be one of the first EMP dedicated experiments

This project has received funding from the *European Union's Horizon 2020 research and innovation programme* under grant agreement No 654220

in a PW class laser facility. This experiment would also be the occasion to test high repetition rate precision stages grounded via a lightning rod system and with no mechanical decoupling and other components to be used at the EUCALL facilities, as for example X-ray detectors to be used at the HED instrument of European XFEL.

5. Conclusions

This activity, performed in the frame of the EUCALL HIREP work package, was mainly aimed at collecting information on EMP mitigation strategies and on the effects of radiated EMP and return currents on high repetition rate precision positioning stages. This activity was required since mitigation strategies used in currently operating facilities for stages at lower repetition rates are either not reliable or not fast enough.

Competence on EMP mitigation strategies have been developed at facilities to enable experimental activities, however most knowledge is anecdotal and mainly not published. In addition, to the best of our knowledge, no overview on EMP generation in high power and high-energy laser experiments has ever been published. Therefore, we provided an overview of the current understanding of EMP emission and of recently published experimental results, along with a brief discussion of the dependence of EMP on experimental parameters (Section 3.1). We also described instruments and methods currently used for EMP and return current measurement is (Section 3.2) and the results of a systematic investigation of emitted EMP performed at the DRACO 150 TW/1 PW facility (see Section 3.3). Finally, we discussed EMP mitigation strategies both for target positioning stages and controllers and for other electronic components (Section 3.4).

6. Acknowledgements

The authors thank all the participants to the EUCALL HIREP EMP Workshop held in Dresden (28-29 August 2017) for productive discussions and for contributing to this report: A. Berghäuser, Ph. Bradford, A. Ferrari, D. Neely, T. Kluge, K. Knöfel, M. Molodtsova, B. Odložilík, P. Raczka, L. Volpe and D. Watts. Support of the HZDR particle acceleration and HED groups is acknowledged: A. Irman, J. Metzkes, H-P. Schlenvoght, K. Zeil, U. Schramm and T. E. Cowan. Support of the HED team of European XFEL is acknowledged: S. Göde, M. Makita. Finally, the authors would like to thank K. Nelissen and B. Zielbauer for fruitful discussions.

7. References

S. Barbarino and F. Consoli, IEEE Trans. Antennas Propag. 58, 4074 (2010).

R. F. Benjamin, G. H. McCall, and A. W. Ehler, Phys. Rev. Lett. 42, 890 (1979).

C. G. Brown, Jr., E. Bond, T. Clancy, S. Dangi, D. C. Eder, W. Ferguson, J. Kimbrough, and A. Throop, J. Phys.: Conf. Ser. 244, 032001 (2010).

C. G. Brown, J. Ayers, B. Felker, W. Ferguson, J. P. Holder, S. R. Nagel, K. W. Piston, N. Simanovskaia, A. L. Throop, M. Chung, and T. Hilsabeck, Rev. Sci. Instrum. 83, 10D729 (2012).

This project has received funding from the *European Union's Horizon 2020 research and innovation programme* under grant agreement No 654220

D. Carroll, Margaret Read, Matthew Selwood, Pascal Jones, Graeme Scott, Robbie Wilson, Paul McKenna, David Neely, Vulcan Petawatt EMP Studies: Oral Presentation at the 2nd EMP Workshop, Warsaw (2017)

J. Cikhardt, J. Krása, M. De Marco, M. Pfeifer, A. Velyhan, E. Krouský, B. Cikhardtová, D. Klír, K. Rezác, J. Ullschmied, J. Skála, P. Kubeš, and J. Kravárik, Rev. Sci. Instrum. 85, 103507 (2014).

COMSOL documentation

http://cdn.comsol.com/documentation/5.0.1.276/IntroductionToCOMSOLMultiphysics.pdf

F. Consoli, R. De Angelis, P. Andreoli, G. Cristofari, and G. Di Giorgio, Phys. Proc. 62, 11 (2015).

Consoli F. et al., Proceedings of the IEEE 15thInternational Conference on Environment and Electrical Engineering (EEEIC), IEEE 182–187 (2015)

F. Consoli, R. De Angelis, L. Duvillaret, P. L. Andreoli, M. Cipriani, G. Cristofari, G. Di Giorgio, F. Ingenito and C. Verona, Sci. Reports 6, 27889 (2016)

M. De Marco, M. Pfeifer, E. Krousky, J. Krasa, J. Cikhardt, D. Klír, and V. Nassisi, J. Phys.: Conf. Ser. 508, 012007 (2014).

M. De Marco, J. Cikhardt, J. Krása, A. Velyhan, M. Pfeifer, E. Krouský, D. Klír, K. Rezác, J. Limpouch, D. Margarone, and J. Ullschmied, Nukleonika 10, 1515 (2015).

M. De Marco, J. Krása, J. Cikhardt, M. Pfeifer, E. Krouský, D. Margarone, H. Ahmed, M. Borghesi, S. Kar, L. Giuffrida, R. Vrana, A. Velyhan, J. Limpouch, G. Korn, S. Weber, L. Velardi, D. Delle Side, V. Nassisi, and J. Ullschmied, J. Instrum. 11, C06004 (2016).

M. De Marco, J. Krása, J. Cikhardt, A. Velyhan, M. Pfeifer, R. Dudžák, J. Dostál, E. Krouský, J. Limpouch, T. Pisarczyk, K Kalinowska, T. Chodurowski, J. Ullschmied, L. Giuffrida, D. Chatain, J.-P. Perin, and D. Margarone, Phys. Plasmas 24, 083103 (2017)

J.-L. Dubois, F. Lubrano-Lavaderci, D. Raffestin, J. Ribolzi, J. Gazave, A. Compant La Fontaine, E. d'Humiéres, S. Hulin, Ph. Nicolaï, A. Poyé, and V. T. Tikhonchuk, Phys. Rev. E 89, 013102 (2014).

D. C. Eder, A. Throop, C. G. Brown, Jr., J. Kimbrough, M. L. Stowell, D. A. White, P. Song, N. Back, A. MacPhee, H. Chen, W. DeHope, Y. Ping, B. Maddox, J. Lister, G. Pratt, T. Ma, Y. Tsui, M. Perkins, D. O'Brien, P. Patel, LLNL-TR-411183 (2009)

F. S. Felber, Appl. Phys. Lett. 86, 231501 (2005).

S. Garcia, D. Chatain and J.-P. Perin, Laser Part. Beams 32, 4 (2014)

S. Kar, H. Ahmed, R. Prasad, M. Cerchez, S. Brauckmann, B. Aurand, G. Cantono, P. Hadjisolomou, C. L. S. Lewis, A. Macchi, G. Nersisyan, A. P. L. Robinson, A. M. Schroer, M. Swantusch, M. Zepf, O. Willi & M. Borghesi, Nat. Comm. 7, 10792 (2016)

J.Krasa, D. Delle Side, E. Giuffreda, V. Nassisi. Characteristics of target polarization by laser ablation, Laser Part. Beams 33 601 (2015)

This project has received funding from the *European Union's Horizon 2020 research and innovation programme* under grant agreement No 654220

J. Krása, J. Cikhardt, M. De Marco, D. Klír, A. Velyhan, K. Rezac, M. Pfeifer, E. Krousky, J. Skala, R. Dudzak, J. Dostal, J. Kaufman, J. Ullschmied, and J. Limpouch, EPS Conf. Plasma Phys. P1.083 (2016).

J. Krása et al, Plasma Phys. Contr. Fus. 59, 065007 (2017)

P. Mora, Phys. Rev. Lett. 90, 185002 (2003).

A. Poyé, S. Hulin, M. Bailly-Grandvaux, J. L. Dubois, J. Ribolzi, D. Raffestin, M. Bardon, F. Lubrano-Lavaderci, E. d'Humiéres, J. J. Santos, P. Nicolaï, and V. Tikhonchuk, Phys. Rev. E 91, 043106 (2015).

A. Poyé, J.-L. Dubois, F. Lubrano-Lavaderci, E. d'Humières, M. Bardon, S. Hulin, M. Bailly-Grandvaux, J. Ribolzi, D. Raffestin, J. J. Santos, Ph. Nicolaï, and V. Tikhonchuk, Phys. Rev. E 92, 043107 (2015).

P. Rączka, J.-L. Dubois, S. Hulin, V. Tikhonchuk, M. Rosiński, A. Zaraś-Szydłowska, and J. Badziak, Proceedings of the 44th EPS Conference on Plasma Physics, P5.213 (2017)

J. L. Remo, R. G. Adams, and M. C. Jones, Appl. Opt. 46, 6166 (2007).

T. S. Robinson, F. Consoli, S. Giltrap, S. J. Eardley, G. S. Hicks, E. J. Ditter, O. Ettlinger, N. H. Stuart, M. Notley, R. De Angelis, Z. Najmudin and R. A. Smith, Sci. Reports 7, 983 (2017)

K. Zeil, J. Metzkes, T. Kluge, M. Bussmann, T. E. Cowan, S. D. Kraft, R. Sauerbrey, B. Schmidt, M. Zier and U. Schramm, Plasma Phys. Conf. Fus., 56 (2014)

8. Publications

I. Prencipe, J. Fuchs, S. Pascarelli, D. Schumacher, R. Stephens, N. Alexander, … T. Cowan, Targets for high repetition rate laser facilities: Needs, challenges and perspectives. High Power Laser Science and Engineering, **5** (2017). doi:10.1017/hpl.2017.18

A review paper on EMP generation and mitigation is in preparation, as a result of the HIREP-EMP Workshop held at HZDR (August 28-29, 2017).

This project has received funding from the *European Union's Horizon 2020 research and innovation programme* under grant agreement No 654220